GEOLOGICA CARPATHICA, AUGUST 2021, 72, 4, 285–298 https://doi.org/10.31577/GeolCarp.72.4.1

Decompression textures in garnet–cordierite gneiss from Kosavankovilpatti, Southern India: Constraints from reaction textures and phase equilibria modelling

ROOPALI YADAV[1], DIVYA PRAKASH[1,✉], SWAPNIL KUMAR RAI[1], MANOJ K. YADAV[2], PRADIP KUMAR SINGH[1] and SRISHTI JAISWAL[1]

[1]Department of Geology (Centre of Advanced Study), Institute of Science, Banaras Hindu University, Varanasi – 221005, India; ✉dprakashbhu@gmail.com
[2]Centre of Advanced Study in Geology, University of Lucknow, Lucknow – 226007, India

(Manuscript received January 8, 2021; accepted in revised form June 10, 2021; Associate Editor: Marian Janák)

Abstract: The Kosavankovilpatti area consists mainly of granulite facies rocks and is part of the Madurai block in the Southern Granulite Terrane, India. The garnet–cordierite gneiss collected at this location exhibits well-preserved metamorphic reaction textures and is used to infer the metamorphic history of the study area. Garnet resorption at the expense of orthopyroxene–cordierite and spinel–cordierite symplectites characterize the retrograde stages of metamorphism. Phase relationships for bulk rock composition in the MnO–Na_2O–CaO–K_2O–FeO–MgO–Al_2O_3–SiO_2–H_2O–TiO_2 (MnNCKFMASHT) system, as well as the application of multi equilibrium calculations for the peak metamorphic assemblages, yield maximum temperature (*T*) and pressure (*P*) conditions of 900 °C and 9 kbar, respectively. These estimated results are lower compared to those reported for the sapphirine-bearing granulites from the Madurai block that characterize UHT metamorphism. The post-peak *P–T* path, constructed for garnet-cordierite gneiss based on observed microstructural relationships and thermobarometry results, is characterized by a decompressive *P–T* segment ending at 810 °C and 5.5 kbar. The geochronological results of SHRIMP U–Pb give an age of 521±30 Ma for the decompression metamorphic overprint that was superimposed on the protolith formation of the garnet–cordierite gneiss at 2561±72 Ma. The proposed *P–T* path implies that the granulites in the Kosavankovilpatti section probably resulted from denudation of the thickened continental crust. In this way, the present study allows us to understand how this part of the lower continental crust could have evolved during prolonged heating without actually attaining UHT conditions.

Keywords: Madurai Block, SHRIMP, Southern Granulite Terrane (SGT), charnockite, Perple_X, garnet–cordierite gneiss.

Introduction

The Southern Granulite Terrane (SGT), found in the southernmost part of the Indian subcontinent of Asia, is one of the few terranes in the world that has preserved the Archean and Proterozoic crust with extensive granulite facies rocks of high-grade. It represents a classic terrane of the Archean continental crust where, due to differential uplift and erosion, as well as tectonic fragmentation, different crustal levels of the crust are exposed. The SGT is composed of several granulite blocks (e.g., Trivandrum block, Madurai block, Nilgiri block, etc.) that are separated by shear/suture zones. The Madurai block (MB) is the largest crustal block of the SGT, and is delimited to the north by the Palghat–Cauvery suture zone (PCSZ) running approximately E–W and to the south by the Achankovil Suture Zone with a NW–SE trend (ASZ) (Santosh 2020). The MB covers the largest area of the SGT and is also related to crust evolution and ultrahigh temperature (UHT) metamorphism (Mohan 2003; Sajeev et al. 2004; Teale et al. 2011; Santosh et al. 2017). The dominant magmatic lithologies in the MB are hornblende biotite gneisses (TTG), charnockites and their intermediate enderbitic rocks, diorites, minor gabbros (including mafic granulites), pink and grey granitoids, pinkish and greyish granites, and pegmatites. The metasedimentary units are represented by garnet–biotite gneiss, garnet–biotite–sillimanite gneiss, quartzites, and metacarbonates (e.g., Santosh et al. 2009).

The highland areas (~1000 m elevation) in the MB consists of charnockite massifs (includes charnockites which is an alkali granitic rock, charno-enderbites and enderbites which is charnockitic tonalite) and the low-lying regions (~600 m elevation) expose orthogneisses, paragneisses and granitic intrusives.

Cenki & Kriegsman (2005) suggested that the SGT has gone through a complex history since the early Proterozoic times, but the only metamorphic event observed in the area so far is of Pan-African age (Jayananda et al. 1995; Ghosh 1999). The SGT most likely formed part of East Gondwana and underwent polyphase ductile deformation and metamorphism during the Pan-African Orogeny in ca. 550–580 Ma (Bartlett et al. 1998; Braun & Kriegsman 2003). During this event, many rocks reached granulite facies conditions (Braun et al. 1996; Chacko et al. 1996; Cenki et al. 2002). The SGT, south of the Dharwar Craton, is a collage of crustal blocks including the Coorg, Nilgiri, Salem, Madras, Madurai, Trivandrum and Nagercoil blocks, where the basement rocks vary in age from

the Mesoarchean to Neoproterozoic (Clark et al. 2009; Collins et al. 2014; Plavsa et al. 2014; Amaldev et al. 2016; Santosh et al. 2016).

The granulites found throughout the study area show several disequilibrium reaction textures that are most promising because they represent distinct segments of the *P–T* path during the metamorphism of the granulite facies. Such a study of texture is important because the South Indian shield granulites are generally thought to be polymetamorphic and have a multi-deformational history. In this contribution, we present the petrographic, mineral chemistry and geochronological data for a newly recognized locality, named Kosavankovilpatti, which is situated in the lower eastern part of the MB. Isothermal decompression within a clockwise *P–T* path could have been associated with the formation of a Large Hot Orogen (LHO).

Geological setting

The MB comprises dominantly charnockite massifs intercalated with elongated narrow belts of metasedimentary rocks including quartzites and cordierite granulites (Tang et al. 2017). Garnet–cordierite–sillimanite gneisses in the Madurai Block have been reported to occur as bands along the Kodaikannal and Madurai regions (Prakash 1999). MB is well-known for high-grade metapelitic granulite rocks and gneisses that form as enclaves within intense migmatites. These rocks serve as robust evidence of UHT metamorphism by retaining sections of the deep Precambrian continental crust of polydeformed igneous and high-grade metamorphic rocks from Archean to Neoproterozoic. The basement is composed of a closely interbanded sequence of felsic, mafic, and ultramafic supracrustal rocks, as well as metasedimentary rocks derived from pelitic, psammitic and calcareous protolith(s) within the charnockites as folded belts (Harris et al. 1982; Drury et al. 1984; Subba Rao et al. 1995; Mohan et al. 1996; Prakash 1996).

The study area (10°15’38”N, 77°31’26”E to 10°22’7”N, 77°34’40”E) is positioned at the base of the southern slope of the Palani Hills, located ~40 km NW of the city of Madurai and continuing as a hilly range beyond Kodaikanal (Fig. 1). The “Upper Palani Hills” encompass the Annamalai, Palani and Cardamom Hills, making them the largest block of highland granulites in southern India. The Upper Palani Hills cover an area of 170 sq. km with an average elevation of 2800 m above the mean sea level. The contact zone of the metasedimentary sequence and the massive charnockites coincides with the eastern margin of the Upper Palani Hills. In this subvertical contact zone, the metapelites are represented by cordierite–garnet–spinel–sillimanite migmatites and further east of this contact zone, garnet–sillimanite–biotite gneisses (khondalites) predominate. Khondalites are found interlayered with calc-silicate rocks, quartzites, pelitic schists and conformable mafic–ultramafic layers.

Earlier workers (e.g., Subba Rao et al. 1995, 1997) who mapped the area around Kosavankovilpatti found, quartzites, charnockites, khondalites, sapphirine-bearing granulites, calc-silicate rocks, leptynites, garnet–cordierite–sillimanite–biotite gneisses, and ultramafic rocks. The garnet–cordierite gneiss rocks exposed in the study area are medium (0.75 to 1 mm) to coarse-grained (1–2 mm), composed of quartz, feldspar and biotite with occasionally orthopyroxene and garnet. The rare presence of orthopyroxene suggests that these rocks should be called migmatitic charnockites rather than gneisses in general. Aggregates of blue granular cordierite and coarse biotite flakes, along with sillimanite needles that define the foliation, are visible in the garnet–cordierite gneiss outcrop (Fig. 2).

Typical metamorphic bands are exhibited alternating melanocratic layers dominated by garnet, orthopyroxene, cordierite, and biotite and leucocratic layers dominated by quartz and feldspar.

Textural relations and interpretation of metamorphic reactions

The garnet–cordierite gneiss from the Kosavankovilpatti area is mainly composed of the following mineral assemblages:

D-1 Orthopyroxene–cordierite–biotite–plagioclase–perthite–quartz±spinel
D-2 Garnet–cordierite–biotite–plagioclase–potash feldspar–quartz–sillimanite±spinel
D-3 Biotite–cordierite–quartz–plagioclase–potash feldspar–garnet±spinel
D-4 Garnet–biotite–cordierite–sillimanite–plagioclase–quartz

In addition to the minerals mentioned above, the assemblages also include small amounts of magnetite, apatite, zircon, and rutile.

The garnet porphyroblasts in garnet–cordierite gneiss are highly fractured and show iron leaching along the fracture planes. Orthopyroxene–cordierite symplectites and pseudomorphs replace the resorbed garnet. In some places, green chlorite can be observed on the margins of the garnet, possibly as a result of retrograde metamorphism. This garnet breakdown reaction is, in general, indicative of isothermal decompression, as also experimentally studied by Hensen & Green (1972) in the FMASH system (e.g., Harley 1989).

The presence of inclusions of biotite, quartz and sillimanite in megacrystic garnet and potash-feldspar (Fig. 3a) can be described by the following prograde reaction:

$$\text{Biotite}+\text{Sillimanite}+2\ \text{Quartz}=\text{Garnet}+\text{Potash-feldspar}+\text{Vapour} \quad (1)$$

The above reaction may be responsible for the garnet formation.

Another important garnet growth reaction can be (Fig. 3b):

$$3\ \text{Spinel}+5\ \text{Quartz}=\text{Garnet}+2\ \text{Sillimanite} \quad (2)$$

The above reactions can be followed by garnet resorption resulting from continuous reactions:

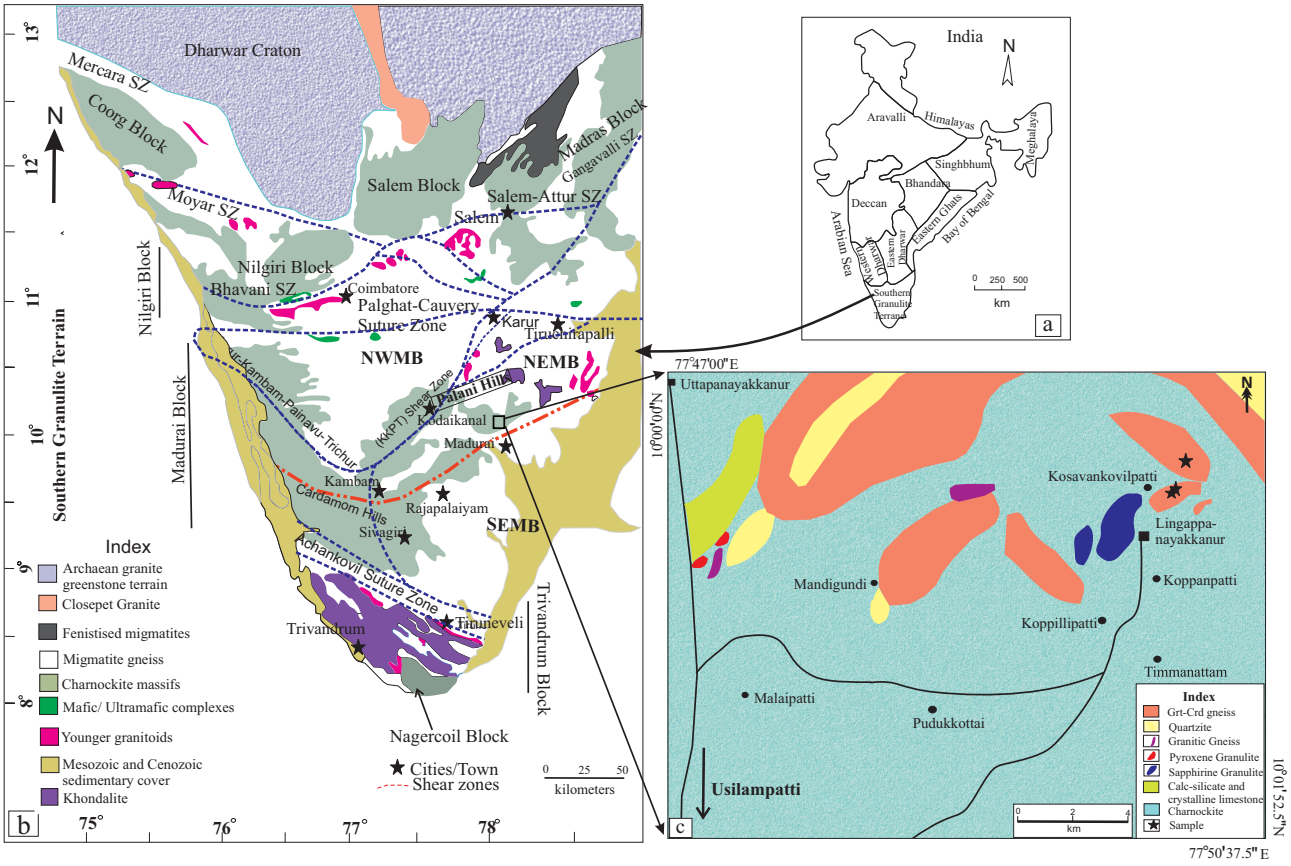

Fig. 1. a — Reference map of India; **b** — Map of southern India modified after Collins et al. 2014. NEMB=North-East Madurai Block, NWMB=North-West Madurai Block, SEMB=South-East Madurai Block; **c** — Geological map of the study area around Kosavankovilpatti near Usilampatti.

2 Garnet+6 Sillimanite=3 Spinel+3 Cordierite (3)
2 Garnet+4 Sillimanite+5 Quartz=3 Cordierite (4)
2 Garnet+3 Quartz=2 Orthopyroxene+3 Cordierite (5)

The development of symplectites of spinel–cordierite (Fig. 3c) and cordierite–orthopyroxene symplectites (Fig. 3d, and e) constitutes the textural evidence for reactions (3) to (5), which are characteristic of isothermal decompression (Hensen & Green 1972; Harley 1989). Reactions (4) and (5) have been experimentally investigated by Richardson (1968) and Holdaway & Lee (1977) in the FASH system.

In some places, green chlorite can be seen on the margins of cordierite–orthopyroxene symplectites (Fig. 3e), providing evidence of retrogression. Only some of the samples showed evidence of retrograde hydration, reflected by biotite and biotite–quartz symplectite replacing orthopyroxene (Fig. 3g, h) via the reaction:

3 Orthopyroxene+K-feldspar+Vapour=Biotite+3 Quartz (6)

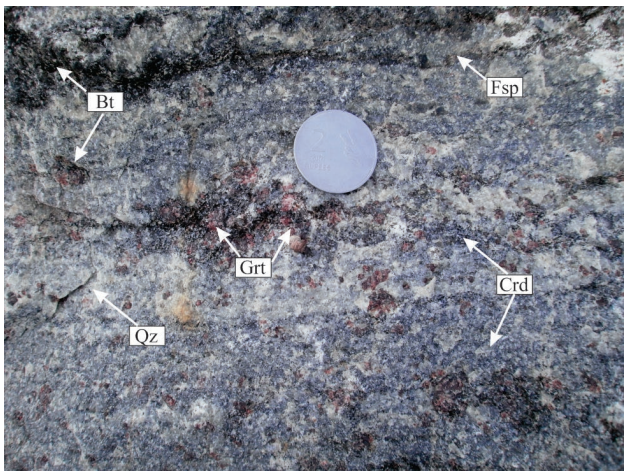

Fig. 2. Garnet–cordierite gneiss outcrop from Kosavankovilpatti showing coarse-grained aggregates of garnet (Grt), cordierite (Crd), quartz (Qz), biotite (Bt) and K-feldspar (Kfs).

Mineral chemistry

The experimental work was carried out in the Electron Probe Micro Analyser (EPMA) CAMECA SXFive instrument at the DST-SERB National Facility, Department of Geology (Centre of Advanced Study), Institute of Science, Banaras Hindu University. The CAMECA SXFive instrument was operated by SXFive Software at a voltage of 15 kV and a current 10 nA with a LaB6 source in the electron gun for

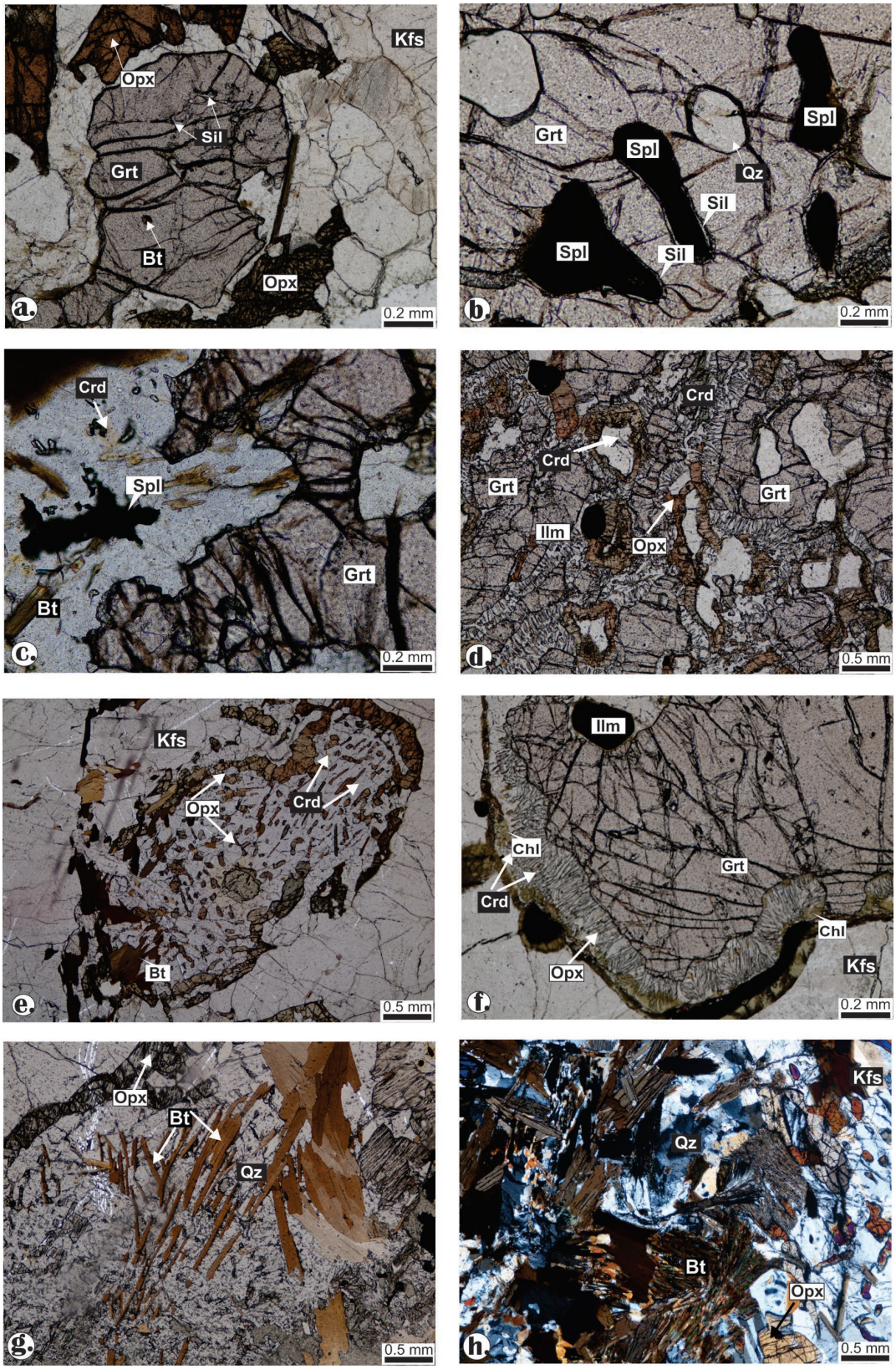

Fig. 3. Photomicrographs illustrating textural relations in the garnet–cordierite gneiss under plane polarized light (PPL): **a** — Inclusions of sillimanite (Sil), quartz & corroded biotite (Bt) in garnet (Grt) porphyroblast; **b** — Spinel & quartz occurring as inclusions in corroded garnet (grt); **c** — Cordierite–spinel symplectite around garnet; **d** — Symplectite of orthopyroxene & cordierite forms rims around the porphyroblastic garnet; **e** — Symplectitic intergrowth of orthopyroxene–cordierite; **f** — Retrogressed green chlorite at the margins of cordierite–orthopyroxene symplectites; **g** — Intergrowth of biotite–quartz near orthopyroxene; **h** — Intergrowth of biotite–quartz (between XP).

the generation of the electron beam. Representative microprobe analyses of various minerals are listed in Table 1. Mineral abbreviations are after Whitney & Evans (2010).

The garnet in the rocks studied is essentially a solid solution between almandine and pyrope with a low content of grossular and spessartine. The core and rim compositions of the porphyroblastic garnet were determined by spot analysis. In the core, the X_{Mg} [Mg/(Mg+Fe^{2+})] values range from 0.54 to 0.56. At the rim, the X_{Mg} values range from 0.43 to 0.50.

The X_{Mg} of biotite ranges from 0.69 to 0.73. Its Ti content is high, ranging between 0.34 to 0.62 atoms per formula unit (apfu). The X_{Mg} of orthopyroxene ranges from 0.64 to 0.68. The orthopyroxene in the matrix is more aluminous (Al_2O_3 >5 wt. %) than the symplectitic orthopyroxene (Al_2O_3<5 wt.%). A decrease in $A1_2O_3$ from the core to the rim is usually concomitant with an increase in MgO, FeO and SiO_2 (Arima & Barnett 1984). X_{Ca} [Ca/(Ca+K+Na)] in plagioclase varies between 0.28 and 0.43. Symplectitic plagioclase shows a relatively higher CaO content (>7 wt. %). Spinel is largely a solid solution between spinel ($MgAl_2O_4$) and hercynite ($Fe^{2+}Al_2O_4$) with an average X_{Mg} of 0.43. The Fe^{3+} content in spinel ranges from 0.04 to 0.11 apfu. Cordierite is consistently richer in magnesium than the coexisting phases. The X_{Mg} ranges from 0.67 to 0.89. No significant compositional zoning was observed in cordierite. Negligible amounts of Na_2O, K_2O and, to a lesser extent, CaO were found in cordierite.

Phase equilibria modelling

To constrain the history of the garnet–cordierite gneiss (sample no. U1528) of the Kosavankovilpatti area, the *P–T* pseudosection (Fig. 4) relevant to the mineral assemblages preserved in these rocks in the MnO–Na_2O–CaO–K_2O–FeO–MgO–Al_2O_3–SiO_2–H_2O–TiO_2 (0.09–1.04–1.47–2.83–11.84–10.88–12.90–55.37–2.30–1.74 wt. %) system was estimated from the whole rock composition. The *Perple_X software* (version 6.8.7), which is based on Gibbs free energy minimization (Connolly 1990, 2005, 2009; Connolly & Petrini 2002) was used to calculate the compositions of mineral assemblages as a function of pressure and temperature. The thermodynamic data set and the internally consistent equation of state for H_2O from Holland & Powell (1998, revised 2004) were used in the calculation of the pseudosections. The detailed formula, notation and sources of the solution models are given in Table 2.

XRF analyses of representative rock samples from the study area were carried out on Siemens SRS-3000 (WD-XRF) in the X-ray fluorescence laboratory, Wadia Institute of Himalayan Geology, Dehradun, India. The amount of H_2O used for *P–T* pseudosection calculations was approximated by the 'loss on ignition' (LOI) value in the bulk analysis. The pressure and temperature ranges selected for modelling of phase equilibria are 4–11 kbar and 327–1027 ºC. The phases and corresponding phase components (in parentheses) chosen are: garnet (alm, py and gr), orthopyroxene (en and fs), cordierite (crd, hcrd and fcrd), K-feldspar (san, mic), plagioclase (ab), biotite (phl, ann and east), ilm, rutile and silicate melt phase (sil8L and q8L). Sillimanite and quartz are taken as pure phases. The solution models (details in solut_08.dat; Perple_X 6.8.7; database: hp02ver.dat) adopted are Gt(JH), Opx(W), Crd(W), Bi(W), and FspC1(W) (Table 2). Isopleths representing the composition of garnet X_{Mg}, orthopyroxene X_{Mg}, biotite X_{Mg} and cordierite X_{Mg} are shown in Fig. 4. The textures and mineral composition data suggest the following peak mineral assemblage: orthopyroxene, garnet, biotite, cordierite and K-feldspar. The development of spectacular orthopyroxene–cordierite and orthopyroxene–spinel–cordierite was followed by cooling during which biotite–quartz symplectites were formed. The *P–T* path has been (represented by large arrow in Fig. 4) drawn based of the calculated isopleths and measured mineral chemistry obtained by EPMA. The *P–T* conditions derived from the simultaneous X_{Mg} isopleth plot of garnet, cordierite, biotite, and orthopyroxene are approximately 880 °C at 8.2 kbar.

The *P–T* condition obtained from the mineral core and symplectite positions of garnet–cordierite gneiss with the *THERMOCALC* program (Holland & Powell 1998) for sample no. 1528 are 890 ºC and 8.7 kbar (core) and 810 °C and 5.5 kbar (symplectite). The *THERMOCALC* results based on the intersection of four possible independent reaction equilibria for the selected phases of the end-member of the sample are given in Table 3.

Geochronology

Backscattered images (BSE) of zircons obtained from garnet–cordierite gneiss (Fig. 5a) reveal that the zircon grains are sub-prismatic and slightly rounded with a size that varies from 150 μm to 250 μm and have a complex and inhomogeneous internal structure. U–Pb analyses of zircon grains were carried out on the Sensitive High Resolution Ion Microprobe (SHRIMP II) at the Activation Laboratories, Canada. Two grains show irregular shaped nucleus and overgrowths. Zircon rims are fairly thick and have oscillatory zoning and suggest that they have experienced different episodes of metamorphic growth in contrast to the cores. Eleven U–Pb spot analyses were carried out on two zircon grains from sample U1528 (Table 4 and Fig. 5a). Analyses plotted as radiogenic ratios, corrected for common ^{204}Pb and shown as two-σ error ellipses. The Wetherill (1956) Concordia plots have been prepared using ISOPLOT/EX (Ludwig 2012; Fig. 5b). The discordant analyses follow a line on a Concordia diagram (Fig. 5b) with an upper intercept at 2561±72 Ma and a lower intercept at 521±30 Ma (MSWD=34). These ages from two different age domains, the Neoarchean and the Neoproterozoic.

The zircon cores and rims show two sets of different ages in total. The core suggests the age of 2561±72 Ma, indicating that the detrital zircons in the studied granulites may have derived from the Archean cratonic source region, while the isotopic results obtained from the rims indicate a much lower age (521±30 Ma), which can be interpreted as dating the timing of high-temperature metamorphism in MB during

Table 1: Representative microprobe analysis of garnet–cordierite gneiss from the study area.

	Garnet (12 Oxygen basis)								
Sample No.	**U1528**	**U1528**	**U1528**	**U1528**	**U1528**	**U1528**	**U1528**	**U1528**	**U1528**
Spot No.	**713**	**733**	**749**	**750**	**751**	**752**	**775**	**776**	**779**
	R	**R**	**C**	**C**	**R**	**R**	**C**	**R**	**R**
Oxide wt. %									
SiO_2	42.01	40.23	40.44	40.57	39.24	38.24	40.58	40.66	38.80
TiO_2	0.03	0.00	0.00	0.00	0.00	0.00	0.00	0.00	0.00
Al_2O_3	19.39	20.48	22.37	21.63	21.55	20.01	21.89	22.54	21.30
Cr_2O_3	0.10	0.16	0.10	0.15	0.08	3.84	0.06	0.08	0.06
FeO*	23.57	24.58	20.92	20.74	24.25	22.65	21.76	21.40	27.48
MnO	0.04	0.38	0.16	0.22	0.29	0.32	0.21	0.23	0.55
MgO	12.91	12.77	13.90	14.40	12.34	12.99	13.95	13.71	11.12
CaO	1.43	0.88	1.69	1.70	1.64	1.69	1.31	1.22	0.63
Total	*99.47*	*99.49*	*99.58*	*99.41*	*99.39*	*99.73*	*99.77*	*99.83*	*99.93*
Si	3.17	3.06	3.02	3.04	2.99	2.93	3.03	3.03	2.98
Al^{IV}	0.00	0.00	0.00	0.00	0.01	0.07	0.00	0.00	0.02
Al^{VI}	1.73	1.84	1.97	1.91	1.93	1.73	1.93	1.98	1.91
Ti	0.00	0.00	0.00	0.00	0.00	0.00	0.00	0.00	0.00
Cr	0.01	0.01	0.01	0.01	0.00	0.23	0.00	0.00	0.00
Fe^{2+}	1.39	1.47	1.30	1.25	1.48	1.41	1.33	1.33	1.69
Mn	0.00	0.02	0.01	0.01	0.02	0.02	0.01	0.01	0.04
Mg	1.45	1.45	1.55	1.61	1.40	1.48	1.55	1.52	1.27
Ca	0.12	0.07	0.14	0.14	0.13	0.14	0.10	0.10	0.05
X_{Mg}	*0.51*	*0.50*	*0.54*	*0.56*	*0.49*	*0.51*	*0.54*	*0.53*	*0.43*

* Total iron as FeO

$X_{Mg}=Mg/(Mg+Fe^{2+})$

C=Core, R=Rim, S=Symplectite

	Plagioclase (8 Oxygen basis)						
Sample No.	**U1528**	**U1528**	**U1528**	**U1528**	**U1528**	**U1528**	**U1528**
Spot No.	**697**	**698**	**708**	**741**	**742**	**753**	**772**
	C	**C**	**R**	**S**	**S**	**S**	**R**
Oxide wt. %							
SiO_2	59.15	58.80	63.63	59.55	56.24	59.32	60.73
TiO_2	0.00	0.00	0.00	0.00	0.00	0.00	0.00
Al_2O_3	24.62	25.30	23.13	24.92	26.72	24.99	24.37
Cr2O3	0.00	0.08	0.00	0.03	1.14	0.04	0.20
FeO	0.06	0.09	0.02	0.10	0.19	0.04	0.14
MnO	0.02	0.00	0.00	0.00	0.00	0.00	0.00
MgO	0.00	0.00	0.00	0.00	0.00	0.00	0.00
CaO	7.32	7.47	5.40	7.51	9.01	7.60	5.63
Na_2O	7.95	7.89	7.59	7.65	6.52	7.82	8.80
K_2O	0.12	0.10	0.17	0.21	0.14	0.16	0.06
Total	*99.25*	*99.73*	*99.94*	*99.96*	*99.96*	*99.97*	*99.93*
Si	2.67	2.64	2.81	2.66	2.54	2.66	2.71
Al	1.31	1.34	1.20	1.31	1.42	1.32	1.28
Cr	0.00	0.00	0.00	0.00	0.04	0.00	0.01
Ti	0.00	0.00	0.00	0.00	0.00	0.00	0.00
Fe	0.00	0.00	0.00	0.00	0.01	0.00	0.01
Mn	0.00	0.00	0.00	0.00	0.00	0.00	0.00
Mg	0.00	0.00	0.00	0.00	0.00	0.00	0.00
Ca	0.35	0.36	0.26	0.36	0.44	0.36	0.27
Na	0.69	0.69	0.65	0.66	0.57	0.68	0.76
K	0.01	0.01	0.01	0.01	0.01	0.01	0.00
X_{Ca}	*0.34*	*0.34*	*0.28*	*0.35*	*0.43*	*0.35*	*0.26*

* Total iron as FeO

$X_{Ca}=Ca/(Ca+Na+K)$

C=Core, R=Rim, S=Symplectite

	Spinel (4 Oxygen basis)	
Sample No.	**U1528**	**U1528**
Spot No.	**735**	**736**
	R	**C**
Oxide wt. %		
SiO_2	0.00	0.00
TiO_2	0.02	0.00
Al_2O_3	61.36	57.90
Cr_2O_3	0.27	0.24
FeO	27.52	30.43
MnO	0.03	0.00
MgO	10.66	11.10
CaO	0.00	0.17
Na_2O	0.01	0.04
K_2O	0.00	0.06
Total	*99.88*	*99.95*
Si	0.00	0.00
Al	1.96	1.88
Ti	0.00	0.00
Cr	0.01	0.01
Fe^{3+}	0.04	0.11
Fe^{2+}	0.59	0.59
Mn	0.00	0.00
Mg	0.43	0.46
X_{Mg}	*0.42*	*0.44*

* Total iron as FeO

$X_{Mg}=Mg/(Mg+Fe^{2+})$

C=Core, R=Rim, S=Symplectite

Table 1 (continued)

	Orthopyroxene (4 Oxygen basis)					
Sample No.	**U1528**	**U1528**	**U1528**	**U1528**	**U1528**	**U1528**
Spot No.	**728**	**737**	**738**	**745**	**746**	**784**
	R	**R**	**S**	**S**	**C**	**R**
Oxide wt. %						
SiO_2	50.17	48.55	47.49	50.35	51.13	51.01
TiO_2	0.20	0.05	0.18	0.00	0.00	0.04
Al_2O_3	5.68	7.41	8.96	4.60	4.51	2.87
Cr_2O_3	0.00	0.00	0.00	0.08	0.18	0.10
FeO*	20.46	20.51	21.30	22.02	19.98	21.96
MnO	0.17	0.13	0.16	0.05	0.19	0.17
MgO	22.48	22.38	21.46	22.71	23.61	23.53
CaO	0.11	0.08	0.05	0.08	0.14	0.18
Na_2O	0.03	0.00	0.02	0.01	0.02	0.00
K2O	0.00	0.03	0.00	0.00	0.00	0.00
Total	*99.31*	*99.13*	*99.62*	*99.89*	*99.77*	*99.86*
Si	1.86	1.81	1.77	1.87	1.89	1.90
Al^{IV}	0.14	0.19	0.23	0.13	0.11	0.10
Al^{VI}	0.11	0.13	0.17	0.08	0.08	0.03
Ti	0.01	0.00	0.01	0.00	0.00	0.00
Cr	0.25	0.33	0.39	0.20	0.20	0.13
Fe^{3+}	0.00	0.00	0.00	0.00	0.01	0.00
Fe^{2+}	0.64	0.64	0.66	0.68	0.61	0.68
Mn	0.01	0.01	0.01	001	0.01	0.01
Ca	0.00	0.00	0.00	0.00	0.01	0.01
Mg	1.24	1.24	1.19	1.26	1.29	1.30
Na	0.00	0.00	0.00	0.00	0.01	0.01
X_{Mg}	*0.66*	*0.66*	*0.64*	*0.65*	*0.68*	*0.66*

	Biotite (22 Oxygen basis)				
Sample No.	**U1528**	**U1528**	**U1528**	**U1528**	**U1528**
Spot No.	**693**	**739**	**740**	**747**	**748**
	C	**R**	**R**	**C**	**C**
Oxide wt. %					
SiO_2	36.68	36.91	36.45	35.97	36.15
TiO_2	5.29	2.99	3.29	5.42	4.54
Al_2O_3	14.66	15.36	15.92	14.81	15.24
Cr_2O_3	0.11	0.08	0.08	0.21	0.12
FeO	12.07	11.65	11.07	12.11	12.15
MnO	0.00	0.02	0.05	0.00	0.00
MgO	15.86	17.37	17.02	15.34	15.24
CaO	0.01	0.07	0.03	0.02	0.01
Na_2O	0.22	0.20	0.14	0.21	0.23
K_2O	8.80	8.96	8.78	8.66	8.55
Total	*93.68*	*93.62*	*92.83*	*92.75*	*92.23*
Si	5.49	5.52	5.47	5.45	5.49
Al^{IV}	2.51	2.48	2.53	2.55	2.51
Al^{VI}	0.08	0.22	0.29	0.09	0.22
Ti	0.60	0.34	0.37	0.62	0.52
Cr	0.01	0.01	0.01	0.03	0.01
Fe	1.51	1.46	1.39	1.53	1.54
Mn	0.00	0.00	0.01	0.00	0.00
Mg	3.54	3.87	3.81	3.46	3.45
K	1.68	1.71	1.68	1.67	1.66
Na	0.06	0.06	0.04	0.06	0.07
X_{Mg}	*0.70*	*0.73*	*0.73*	*0.69*	*0.69*

* Total iron as FeO

$X_{Mg}=Mg/(Mg+Fe^{2+})$

C=Core, R=Rim, S=Symplectite

	Cordierite (18 Oxygen basis)													
Sample No.	**U1528**	**U1528**	**U1528**	**U1528**	**U1528**	**U1528**	**U1528**	**U1528**	**U1528**	**U1528**	**U1528**	**U1528**	**U1528**	**U1528**
Spot No.	**695**	**696**	**710**	**711**	**714**	**715**	**729**	**730**	**743**	**757**	**758**	**767**	**768**	**782**
	C	**R**	**R**	**R**	**C**	**S**	**R**	**R**	**S**	**R**	**S**	**R**	**R**	**S**
Oxide wt. %														
SiO_2	49.45	49.71	49.24	48.81	50.25	46.99	48.54	48.56	49.20	48.41	48.54	48.41	48.04	48.26
TiO_2	0.00	0.00	0.00	0.00	0.00	0.04	0.04	0.11	0.00	0.00	0.00	0.00	0.07	0.00
Al_2O_3	32.31	33.56	33.06	32.24	5.30	28.77	31.49	33.08	32.28	32.33	32.55	32.44	32.94	32.92
Cr_2O_3	0.12	0.00	0.14	0.04	0.22	0.54	0.15	0.08	0.09	0.00	0.00	0.12	0.00	0.08
FeO	3.37	3.98	3.83	3.35	20.23	2.85	3.48	3.60	3.42	3.56	3.79	3.54	3.56	3.75
MnO	0.00	0.00	0.05	0.00	0.00	0.00	0.00	0.00	0.00	0.00	0.06	0.01	0.00	0.00
MgO	11.69	11.67	11.74	11.77	23.24	10.95	11.09	11.51	11.52	11.46	11.40	11.37	11.26	11.22
CaO	0.01	0.00	0.00	0.00	0.05	0.67	0.04	0.00	0.00	0.00	0.00	0.03	0.02	0.01
Na_2O	0.03	0.03	0.04	0.05	0.02	0.20	0.07	0.03	0.06	0.02	0.03	0.04	0.05	0.03
K_2O	0.00	0.00	0.00	0.00	0.00	0.09	0.04	0.00	0.04	0.00	0.00	0.00	0.00	0.00
Total	*96.97*	*98.96*	*98.09*	*96.26*	*99.31*	*91.09*	*94.94*	*96.98*	*96.60*	*95.78*	*96.37*	*95.97*	*95.94*	*96.28*
Si	5.04	4.98	4.98	5.02	5.59	5.12	5.06	4.96	5.04	5.01	5.00	5.00	4.96	4.90
Fe	0.29	0.33	0.32	0.29	1.88	0.26	0.30	0.31	0.29	0.31	0.33	0.31	0.31	0.32
Al	3.89	3.97	3.94	3.91	0.70	3.69	3.87	3.99	3.90	3.94	3.95	3.95	4.01	4.01
Cr	0.01	0.00	0.01	0.00	0.02	0.05	0.01	0.01	0.01	0.00	0.00	0.01	0.00	0.01
Mn	0.00	0.00	0.00	0.00	0.00	0.00	0.00	0.00	0.00	0.00	0.01	0.00	0.00	0.00
Mg	1.78	1.74	1.77	1.80	3.85	1.78	1.72	1.75	1.76	1.77	1.75	1.75	1.73	1.72
Ca	0.00	0.00	0.00	0.00	0.01	0.08	0.00	0.00	0.00	0.00	0.00	0.00	0.00	0.00
Na	0.01	0.01	0.01	0.01	0.00	0.04	0.01	0.01	0.01	0.00	0.01	0.01	0.01	0.01
X_{Mg}	*0.89*	*0.86*	*0.88*	*0.86*	*0.67*	*0.87*	*0.85*	*0.85*	*0.86*	*0.85*	*0.84*	*0.85*	*0.85*	*0.84*

* Total iron as FeO

$X_{Mg}=Mg/(Mg+Fe^{2+})$

C=Core, R=Rim, S=Symplectite

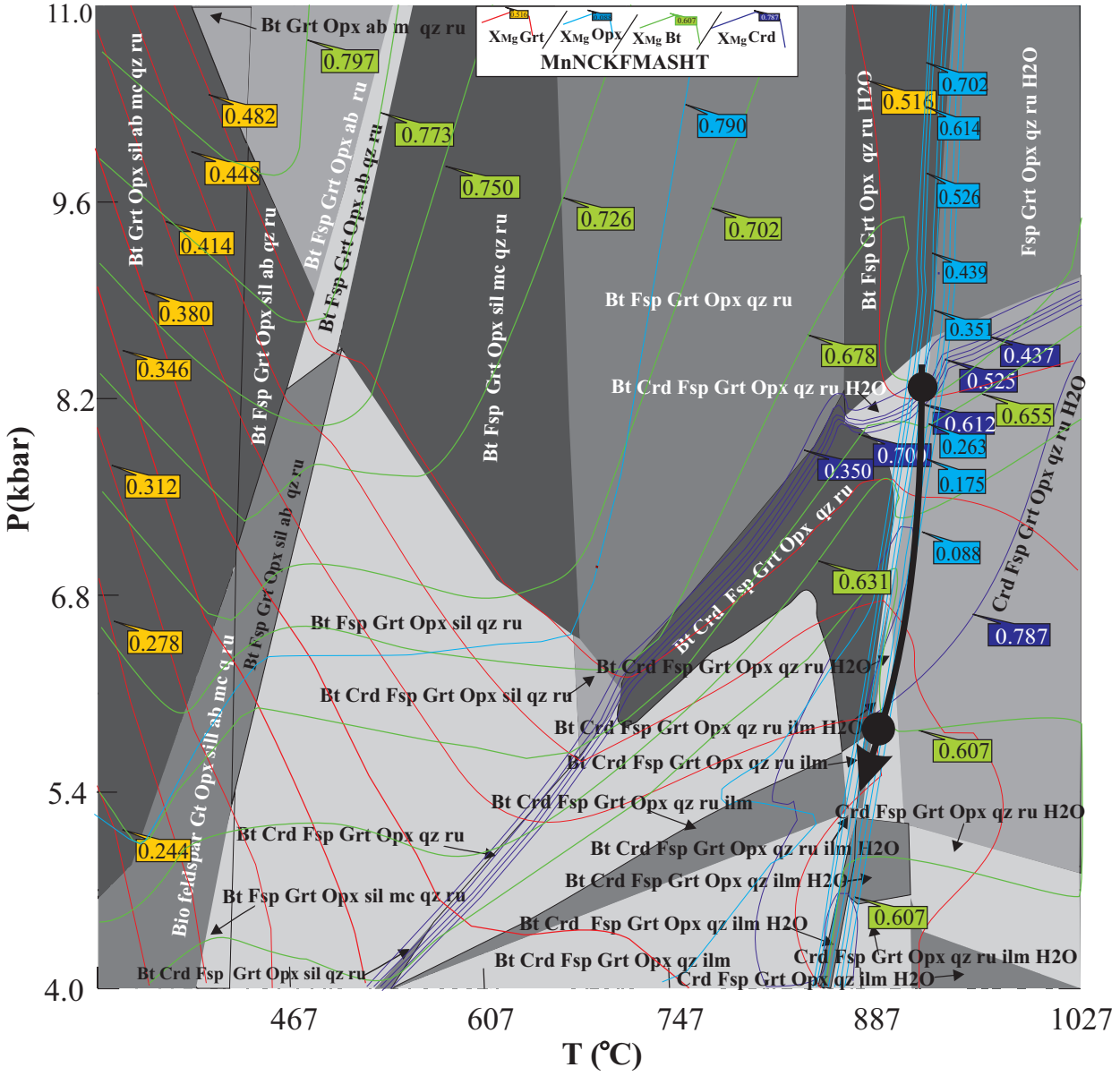

Fig. 4. *P–T* pseudosection calculated for the garnet–cordierite gneiss (sample no. U1528) in the model system MnNCKFMASHT (MnO–Na_2O–CaO–K_2O–FeO–MgO–Al_2O_3–SiO_2–H_2O–TiO_2). Bulk composition in weight % (MnO – 0.09; Na_2O – 1.04; CaO – 1.47; K_2O – 2.83; FeO – 11.84; MgO – 10.88; Al_2O_3 – 12.90; SiO_2 – 55.37; H_2O – 2.30; TiO_2 – 1.74). Calculated X_{Mg} isoplethsare shown for garnet, orthopyroxene, cordierite, and biotite.

the Neoproterozoic. However, the isotopic results extending between 568 Ma and 412 Ma are interpreted as dating, the time of metamorphism in the MB as Neoproterozoic–Cambrian coinciding with the global Pan-African crustal evolution event. It also strengthens the Paleoproterozoic accretion and Pan-African reworking in the MB.

Discussion

Lithologically, the garnet–cordierite gneiss is an important part of the investigation in the MB of the SGT. The modelling of mineral compositions, particularly X_{Mg} isopleths of garnet, cordierite, biotite and orthopyroxene, suggests that the maximum temperatures reached approximately 880 °C at a pressure of 8.2 kbar. Geothermobarometry, with increasing texture evidence, which includes the presence of inclusions of biotite, quartz, and sillimanite within the megacrystic garnet and spinel that is not in contact with the quartz, is indicative of maximum *P–T* conditions of 9 kbar and 900 °C. These conditions suggest that the Kosavankovilpatti granulites formed during prolonged heating of the crust; however, UHT conditions were not reached. Thermobaric calculations for the orthopyroxene–cordierite and spinel–cordierite decompression symplectites at the periphery of the relict garnet, point towards substantial decompression of up to 3 kbar and rapid denudation of

Table 2: Notation of solutions, formulas and model sources for the calculation of pseudosections.

Symbol in Perple_X solution model file	Symbol	Solution Name	Formula	Source
Gt(JH)	Grt	Garnet	$Fe_{3x}Ca_{3y}Mg_{3z}Mn_{3(1-x-y-z)}Al_2Si_3O_{12}$, $x+y+z\leq1$	Jennings & Holland (2015)
Opx(W)	Opx	Orthopyroxene	$[Mg_xFe_{1-x}]2-_yAl_{2y}Si_{2-y}O_6$	White et al. (2014)
Bi(W)	Bt	Biotite	$K[Mg_xFe_yMn_{1-x-y}]_{3-u-v-w}Fe_{3+w}Ti_uA_{l1}+vSi_{3-v}O_{10}(OH)_{2-2u}$, $x+y\leq1$, $u+v+w\leq1$	White et al. (2014)
Crd(W)	Crd	Cordierite	$Mg_{2x}Fe_{2y}Mn_{2(1-x-y)}Al_4Si_5O_{18}\bullet(H_2O)_z$, $x+y\leq1$	White et al. (2014)
FspC1(W)	Fsp	feldspar	$K_yNa_xCa_{1-x-y}Al_{2-x-y}Si_{2+x+y}O_8$, $x+y\leq1$	White et al. (2014)

Table 3: Simultaneous calculation of the pressure–temperature conditions of garnet-cordierite gneiss (sample no. 1528, CORE and SYMPLECTITE) by *THERMOCALC* program and assemblage used Grt–Pl–Opx–Crd–Qz.

Equilibria plotted for CORE	Equilibria plotted for SYMPLECTITE
4 Alm+2 Prp+9 Qz=12 Fs+3 Crd	Alm+fCrd=3 Si+5 Fs
fCrd+4 Fs=3 Qz+2 Alm	3 fCrd+2 Prp=3 Crd+2 Alm
3 fCrd+2 Prp=3 Crd+2 Alm	5 Alm+3 Crd=9 Si+2 Prp+15 Fs
2 fCrd+2 Prp+3 Qz=4 Fs+3 Crd	5 fCrd+2 Prp=6 Si+10 Fs+3 Crd
T (°C)=890, P (kbar)=8.7, sd (T)=80, sd (P)=1.3, cor=0.179, fit=1.35	T (°C)=810, P (kbar)=5.5, sd (T)=69, sd (P)=0.9, cor=0.121, fit=0.77

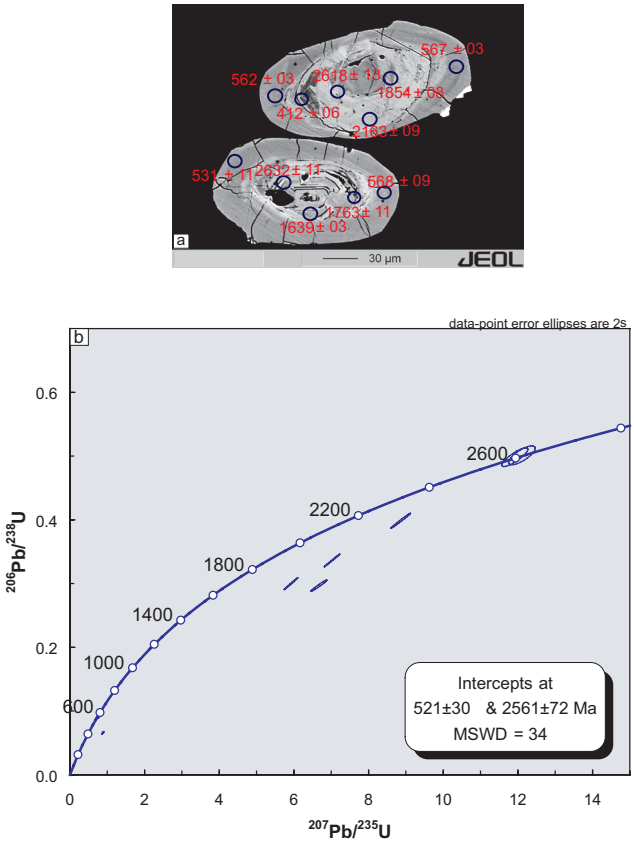

Fig. 5. a — BSE images of zircon grains from garnet–cordierite gneiss; **b** — Wetherill Concordia plot of SHRIMP-II U–Pb zircon analyses for garnet–cordierite gneiss.

the crust, followed by near-isobaric cooling (IBC) during which biotite–quartz symplectites were formed. Although post-peak isobaric cooling and isothermal decompression have been reported in other granulite belts around the world, the orientations of the *P–T* trajectories (clockwise vs. anti-clockwise) require well-constrained granulites *P–T* histories. However, retrograde decompression portions of clockwise *P–T* trajectories have been reported in the adjacent Eastern Ghats Mobile Belt (Lal et al. 1987; Dasgupta et al. 1992; Mohan et al. 1997; Gupta et al. 2000; Prakash et al. 2015) and Eastern Dharwar Craton (Sarvothaman 1984; Sharma et al. 2003; Sharma & Prakash 2007, 2008; Prakash & Sharma 2008, 2011; Prakash et al 2013, 2017; Prakash & Singh 2014). Kelyphite and other symplectite textures are typically form by the breakdown of unstable phases during changes in physical parameters, most commonly pressure. Symplectites can be the decomposition product of a single phase (kelyphite term *sensu stricto* is used in case the primary phase is garnet) or an incomplete reaction product between two adjacent thermodynamically incompatible phases. Even in the absence of generalized deformation, rapid exhumation can produce symplectite textures, particularly when catalysed by deformation and/or fluid influx (Topuz & Altherr 2004). However, detained symplectites (as in the present case made up of orthopyroxene–cordierite and biotite–quartz pairs) may indicate relatively rapid exhumation rates. Symplectites are potential tools for understanding the later parts of the metamorphic history of host rocks, as well as the processes and mechanisms responsible for the formation reactions of symplectite, including those involving open systems (Mongkoltip & Ashworth 1983; Obata 1994, 2011). The decompressive *P–T* trajectory may reflect tectonic denudation after a period of thickening of the crust. However, the exhumation mechanism remains uncertain. Tectonic models for granulite formation that consider the decompressive *P–T* path include (i) thickening of the crust due to continental collision (Thompson & England 1984) and (ii) an extensional regime, involving a crust of near-normal thickness (Sandiford & Powell 1986). The results obtained from forward and backward modelling suggest that the peak *P–T*

Table 4: SHRIMP data for sample U1528.

Spot	% $^{206}Pb_c$	ppm U	ppm Th	$^{232}Th/^{238}U$	ppm $^{206}Pb^*$	(1) $^{206}Pb/^{238}U$ Age	(1) $^{207}Pb/^{206}Pb$ Age	% Discordant	(1) $^{238}U/^{206}Pb^*$	±%	(1) $^{207}Pb^*/^{206}Pb^*$	±%	(1) $^{207}Pb^*/^{235}U$	±%	(1) $^{206}Pb^*/^{238}U$	±%	error
1.1	0.17	574	15	0.03	46.2	567 ±03	593 ±32	5	10.96	2.4	0.0602	2.1	0.765	3.2	0.0924	2.4	.762
1.2	0.19	571	21	0.04	46.7	562 ±03	589 ±32	4	9.96	2.4	0.0589	2.2	0.771	2.4	0.0916	2.4	.753
1.3	0.08	814	127	0.16	224	1763 ±11	2388 ±16	39	3.212	2.4	0.15386	0.67	6.671	2.6	0.2968	2.4	.978
1.4	0.05	689	459	0.67	304	2632 ±11	2612 ±12	−1	1.92	2.4	0.1748	0.93	12.11	2.4	0.5012	2.4	.752
1.5	0.04	213	93	0.44	89	2618 ±13	2594 ±17	−1	2.007	2.4	0.1738	0.83	11.92	2.4	0.4982	2.4	.848
1.6	0.04	1066	116	0.10	356	2163 ±09	2468 ±9	16	2.517	2.4	0.16078	0.36	8.862	2.4	0.3986	2.4	.991
1.7	0.03	692	109	0.16	203	1854 ±08	2353 ±6	23	3.017	2.5	0.1517	0.26	7.021	2.4	0.3362	2.4	.996
1.8	0.02	658	611	0.93	173	1639 ±03	2321 ±9.5	39	3.458	2.5	0.1478	0.34	5.921	2.5	0.2998	2.5	.994
1.9	0.13	373	96	0.26	29.3	568 ±09	553 ±24	−1	10.97	2.4	0.05861	0.13	0.738	2.6	0.0912	2.4	.855
1.10	0.13	239	84	0.35	17.9	531 ±11	524 ±39	−2	11.62	2.4	0.0581	1.9	0.691	3.2	0.0866	2.4	.782
1.11	0.39	1739	179	0.10	100.2	412 ±06	1581 ±11	281	15.41	2.4	0.0976	0.67	0.877	2.4	0.0657	2.4	.967

conditions of the Kosavankovilpatti granulites correspond to a depth of ca. 27 km. The present thickness of the crust under the MB is estimated to be almost 35 km (e.g., Prasad et al. 2007; Naganjaneyulu & Santosh 2011). The slightly rounded zircon grains with discontinuous rims that occur around the cores may be evidence of multiple recycling and polyphase metamorphism mainly during the Archean. Subsequent events during the Pan-African time were attributed to the reworking process. Taking into account the thickness of the underlying crust under the Kosavankovilpatti and adjacent area at the time of Pan-African metamorphism, the total crustal thickness is estimated to be almost 62 km, assuming that no younger tectonism has caused crust thickening by shortening or magma-underplating mechanisms. Therefore, a continent–continent collision may be the best possible mechanism to explain the thickening of the crust, which was followed by decompression.

High temperature metamorphism in the Madurai block: heat source and tectonics

The MB is recognized as a granulite terrane involved in the oblique collision with pre-existing Archean blocks of the Indian peninsula of the time. The orogenic phase (continent–continent collision) of the Pan-African time and the formation of a supercontinent achieved through cratonic amalgam are assumed to cause high-temperature metamorphism in the MB (Tsunogae et al. 2008; Brandt et al. 2011; Fig. 6). High-temperature metamorphism with a clockwise *P–T* trajectory provides the idea of a LHO as a driving force and heat source (Fig. 7). High-temperature metamorphic conditions could be achieved by an abnormally high geothermal gradient (20 °C/Km to 75 °C/km) (Brown 2007; Stüwe 2007). The collision of the SGT with the Archean Dharwar block and the subsequent subduction of the former led to the development of an overly thickened crust (Fig. 7). Crust thickening to form a wide-range tableland that must have survived long enough for enhanced radioactive heating to substantially raise crust temperatures (Clark et al. 2011). Radiogenic heat is believed

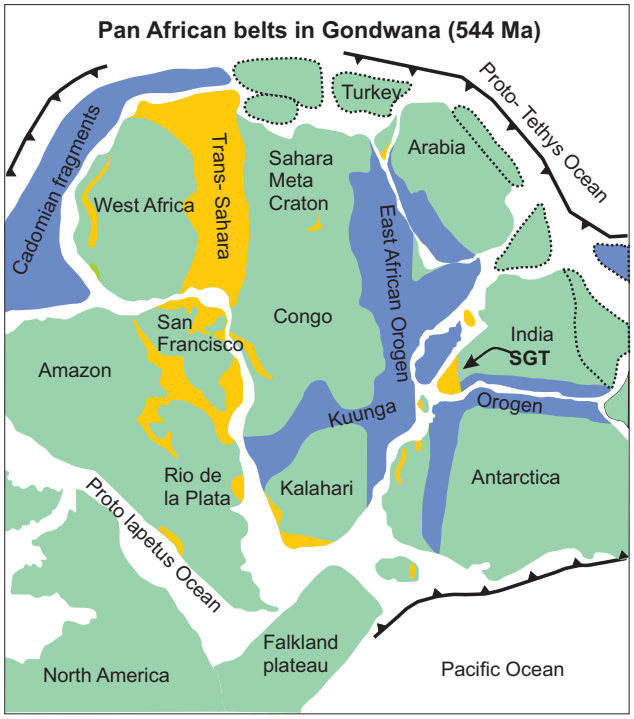

Fig. 6. Paleogeographical reconstruction of Gondwana in the latest Neoproterozoic–Cambrian showing the central position of the SGT within the Gondwana assembly (modified after Brandt et al. 2011).

to be an important factor in heat distribution within the crust (Sandiford & Mclaren 2006; Lei & Xu 2018) and is in a very close approximation to high-temperature metamorphism (Clark et al. 2011, 2015). The deformation in the course of orogenic evolution in the SGT may have resulted in strain heating, in addition to the heat generated due to the thickening of the crust and the radiogenic heat of heat producing elements (HPE). Since deformation heating in ductile shear zones depends on the amount of stress suffered by the lithosphere and the rate of heat transfer from the deformation zone (Nabelek et al. 2010), which decreases rapidly with increasing temperature, the heat is conserved in granulite terranes that undergo deformation (Whittington et al. 2009).

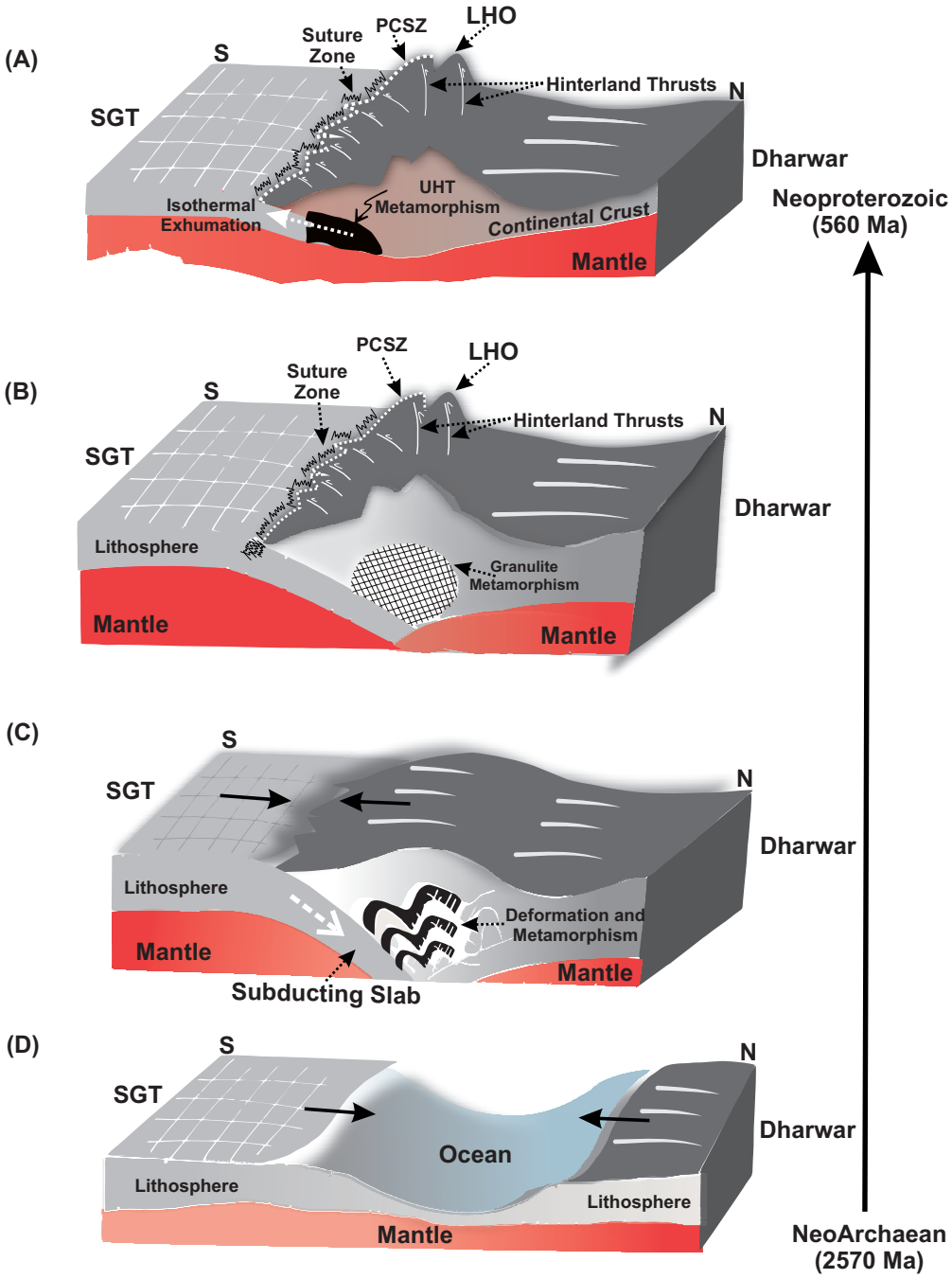

Fig. 7. Schematic model showing the suggested tectonic evolution of the Madurai granulites. PCSZ=Palghat Cauvery Shear Zone, LHO=Large Hot Orogen.

We suggest here that during the course of the granulitization process, the loss of melt that renders the shear zone infertile, causes the lithology to become anhydrous and successive metamorphic processes lead to the formation of granulites. In addition, we suggest here that the sum total of heat emanating from HPE decay plus heat due to lithostatic pressure plus deformation heating should be conserved for a high temperature to be generated, followed by the slow exhumation rate of the granulites, diagnostic of the decompression regime.

Conclusions

The studied mineral–mineral relationships and quantitative analyses in relation to the phase equilibria modelling of the bulk-rock composition in the expanded MnNCKFMASHT system using improved datasets and solution models have provided some new numerical results explaining the rationale behind the metamorphic evolution of high temperature granulites in this part of the granulitic terrane in particular, and

the main, if not entire, part of the SGT, in general. The orthopyroxene–cordierite symplectite rims around the relict garnet indicate decompression of the rocks at high metamorphic temperatures, although the area has been reported to have undergone UHT metamorphism (Prakash et al. 2018). We have discussed the implications of our findings for the tectonic history of the region.

Acknowledgements: This work has been completed through the DST (SERB) research project (P-07-704) to DP and SRF (UGC-BSR) to RY. We also thank the Head of Department of Geology, BHU and the CAS programme of the UGC at BHU for providing the necessary infrastructure facilities. We thank the Editor Prof. Marian Janák and the reviewers Prof. P. Nabelek and anonymous for their helpful comments and suggestions to improve our final version of the manuscript.

References

Amaldev T., Santosh M., Tang L., Baiju K. R., Tsunogae T. & Satyanarayanan M. 2016: Mesoarchean convergent margin processes and crustal evolution: Petrologic, geochemical and zircon U–Pb and Lu–Hf data from the Mercara Suture Zone, Southern India. *Gondwana Research* 37, 182–204. https://doi.org/10.1016/j.gr.2016.05.017

Arima M. & Barnett R.L. 1984: Sapphirine bearing granulites from the Sipiwesk Lake area of the late Archean Pikwitonei granulite terrain. Manitoba Canada. *Contributions to Mineralogy and Petrology* 88, 102–112.

Bartlett J.M., Dougherty-Page J.S. & Harris N.B. 1998: The application of single zircon evaporation & model Nd ages to the interpretation of polymetamorphic terrains: an example from the Proterozoic mobile belt of south India. *Contributions to Mineralogy and Petrology* 131, 181–195. https://doi.org/10.1007/s004100050387

Brandt S., Schenk V., Raith M.M., Appel P., Gerdes A. & Srikantappa C. 2011: Late Neoproterozoic PT evolution of HP-UHT granulites from the Palni Hills (South India): New constraints from phase diagram modelling, LA-ICP-MS zircon dating and in-situ EMP monazite dating. *Journal of Petrology* 52, 1813–1856. https://doi.org/10.1093/petrology/egr032

Braun I. & Kriegsman L. M. 2003: Proterozoic crustal evolution of southernmost India and Sri Lanka. *Geological Society, London, Special Publications* 206, 169–202. https://doi.org/10.1144/GSL.SP.2003.206.01.10

Braun I., Raith M. & Kumar G.R. 1996: Dehydration–melting phenomena in leptynitic gneisses and the generation of leucogranites: a case study from the Kerala Khondalite Belt, southern India. *Journal of Petrology* 37, 1285–1305. https://doi.org/10.1093/petrology/37.6.1285

Brown M. 2007: Metamorphic conditions in orogenic belts: a record of secular change. *International Geology Review* 49, 193–234. https://doi.org/10.2747/0020-6814.49.3.193

Cenki B. & Kriegsman L.M. 2005: Tectonics of the Neoproterozoic southern granulite terrain, South India. *Precambrian Research* 138, 37–56. https://doi.org/10.1016/j.precamres.2005.03.007

Cenki B., Kriegsman L.M. & Braun I. 2002: Melt-producing and melt-consuming reactions in the Achankovil cordierite gneisses, South India. *Journal of Metamorphic Geology* 20, 543–561. https://doi.org/10.1046/j.1525-1314.2002.00388.x

Chacko T., Hu X., Mayeda T.K., Clayton R.N. & Goldsmith J.R. 1996: Oxygen isotope fractionations in muscovite, phlogopite, and rutile. *Geochimica et Cosmochimica Acta* 60, 2595–2608. https://doi.org/10.1016/0016-7037(96)00112-3

Clark C., Collins A.S., Timms N.E., Kinny P.D., Chetty T.R.K. & Santosh M. 2009: SHRIMP U–Pb age constraints on magmatism and high-grade metamorphism in the Salem Block, southern India. *Gondwana Research* 16, 27–36. https://doi.org/10.1016/j.gr.2008.11.001

Clark C., Fitzsimons I.C.W. & Healy D. 2011: How does the continental crust get really hot? *Elements* 7, 235–240. https://doi.org/10.2113/gselements.7.4.235

Clark C., Healy D., Johnson T., Collins A.S., Taylor R.J., Santosh M. & Timms N.E. 2015: Hot orogens and supercontinent amalgamation: A Gondwanan example from southern India. *Gondwana Research.* 28, 1310–1328. https://doi.org/10.1016/j.gr.2014.11.005

Collins A.S., Clark C. & Plavsa D. 2014: Peninsular India in Gondwana: The tectonothermal evolution of the Southern Granulite Terrain & its Gondwanan counterparts. *Gondwana Research* 25, 190–203. https://doi.org/10.1016/j.gr.2013.01.002

Connolly J.A.D. 1990: Multivariable phase-diagrams – an algorithm based on generalized thermodynamics. *American Journal of Science* 290, 666–718.

Connolly J.A.D. 2005: Computation of phase equilibria by linear programming: a tool for geodynamic modeling & its application to subduction zone decarbonation. *Earth And Planetary Science Letters* 236, 524–54. https://doi.org/10.1016/j.epsl.2005.04.033

Connolly J.A.D. 2009: The geodynamic equation of state: what and how. *Geochemistry, Geophysics, Geosystems* 10, Q10014. https://doi.org/10.1029/2009GC002540

Connolly J.A.D. & Petrini K. 2002: An automated strategy for calculation of phase diagram sections & retrieval of rock properties as a function of physical conditions. *Journal of Metamorphic Geology* 20, 697–708.

Dasgupta S., Sengupta P. & Fukuoka M. 1992: Dehydration melting, fluid buffering & decompressional P–T path in a granulite complex from the Eastern Ghats, India. *Journal of Metamorphic Geology* 10, 777–788.

Drury S.A., Harris N.B.W. & Holt R.W. 1984: Precambrian tectonics & crustal evolution in South India. *Journal of Geology* 92, 3–20.

Ghosh J.G. 1999: U/Pb geochronology and structural geology across major shear zones of the southern granulite terrain of India, and organic carbon isotope stratigraphy of the Gondwana coal basins of India. *Doctoral dissertation, Ph. D. dissertation, University of Cape Town*.

Gupta S., Bhattacharya A. & Raith M. 2000: Contrasting pressure–temperature–deformation history across a vestigial craton-mobile belt boundary: the western margin of the Eastern Ghats Belt at Deobhog, India. *Journal of Metamorphic Geology* 18, 683–697. https://doi.org/10.1046/j.1525-1314.2000.00288.x

Harley S.L. 1989: The origins of granulites: a metamorphic perspective. *Geological Magazine* 126, 215–247.

Harris N.B.W., Holt R.W. & Drury S.A. 1982: Geobarometry, geothermometry, & late Archean geotherms from the granulite facies terrain of South India. *Journal of Geology* 90, 509–527.

Hensen B.J. & Green D.H. 1972: Experimental study of cordierite & garnet in pelitic compositions at high pressures & temperatures, II. Compositions without alumino-silicate. *Contributions to Mineralogy and Petrology* 35, 331–354.

Holdaway M.J. & Lee S.M. 1977: Fe–Mg cordierite stability in high grade pelitic rocks based on experimental theoretical & natural observations. *Contributions to Mineralogy and Petrology* 63, 175–193.

Holland T.J.B. & Powell R. 1998: An internally consistent thermodynamic data set for phases of petrological interest. *Journal of Metamorphic Geology* 16, 309–343. https://doi.org/10.1111/j.1525-1314.1998.00140.x

Jayananda M., Janardhan A.S., Sivasubramanian P. & Peucat J.J. 1995: Geochronologic and isotopic constraints on granulite formation in the Kodaikkanal area, southern India. *Memoirs – Geological Society of India* 34, 373–390.

Jenning E.S. & Holland T.J.B. 2015: A simple thermodynamic model for melting of peridotite in the system NCFMASOCr. *Journal of Petrology* 56, 869–892. https://doi.org/10.1093/petrology/egv020

Lal R.K. Ackermand D. & Upadhyay H. 1987: P–T–X relationships deduced from corona textures in sapphirine–spinel–quartz assemblages from Paderu, Southern India. *Journal of Petrology* 28, 1139–1168.

Lei H. & Xu H. 2018: A review of ultrahigh temperature metamorphism. *Journal of Earth Scicences.* 29, 1167–1180. https://doi.org/10.1007/s12583-018-0846-9

Ludwig K.R. 2012: User's Manual for Isoplot 3.75: A Geochronological Toolkit for Microsoft Excel. *Berkeley Geochronology Center Special Publication* 5.

Mohan A. 2003: Granulites & ultrahigh temperature metamorphism: key issues. In: Indian continental lithosphere: emerging research trends. *Memoirs – Geological Society of India* 53, 149–165.

Mohan A., Prakash D. & Motoyoshi Y. 1996: Decompressional P–T history in Sapphirine granulites from Kodaikanal, southern India. *Journal of South American Earth Sciences* 14, 231–243.

Mohan A., Tripathi P. & Motoyashi Y. 1997: Reaction history of sapphirine granulites & a decompressional P–T path in a granulite complex from the Eastern Ghats. *The Proceedings of the Indian Academy of Sciences (Earth & Planetary Sciences)* 106, 115–130.

Mongkoltip P. & Ashworth J.R. 1983: Quantitative estimation of an open-system symplectite-forming reaction: restricted diffusion of Al & Si in coronas around olivine. *Journal of Petrology.* 24, 635–661.

Nabelek P.I., Whittington A.G. & Hofmeister A.M. 2010: Strain heating as a mechanism for partial melting and ultrahigh temperature metamorphism in convergent orogens: Implications of temperature-dependent thermal diffusivity and rheology. *Journal of Geophysical Research* 115, B12. https://doi.org/10.1029/2010JB007727

Naganjaneyulu K. & Santosh M. 2011: Crustal architecture beneath Madurai Block, southern India deduced from magnetotelluric studies: implications for subduction–accretion tectonics associated with Gondwana assembly. *Journal of Asian Earth Sciences* 40, 132–143.

Obata M. 1994: Material transfer & local equilibria in a zoned kelyphite from a garnet pyroxenite, Ronda, Spain. *Journal of Petrology* 35, 271-287.

Obata M. 2011: Kelyphite & symplectite: textural & mineralogical diversities & universality, & a new dynamic view of their structural formation. New Frontiers in Tectonic Research-General Problems. *Sedimentary Basins & Island Arcs* 91-122.

Plavsa D., Collin A. S., Payne J. L., Foden J. D. Clark C. & Santosh M. 2014: Detrital zircons in basement metasedimentary protoliths unveil the origins of southern India. *Bulletin* 126, 791–811.

Prakash D. 1996: Petrology of the granulites from the Kodaikanal-Palani section, Madurai district, Tamil Nadu. *Journal of Scientific Research* 46, 245–251.

Prakash D. 1999: Petrology of the basic granulites from Kodaikanal, South India. *Gondwana Research* 2, 95–104. https://doi.org/10.1016/S1342-937X(05)70130-1

Prakash D. & Sharma I.N. 2008: Reaction textures & metamorphic evolution of quartz-free granulites from Namlekonda (Karimnagar), Andhra Pradesh, Southern India. *International Geology Review* 50, 1008–1021. https://doi.org/10.2747/0020-6814.50.11.1008

Prakash D. & Sharma I.N. 2011: Metamorphic evolution of the Karimnagar granulite terrane, Eastern Dharwar Craton, south India. *Geological Magazine* 148, 112–132.

Prakash D. & Singh P.C. 2014: New finding of sillimanite in sapphirine-bearing granulites from Pedapalli, NE part of the Eastern Dharwar Craton, India. *Journal of Geological Society. India* 84, 29–34.

Prakash D., Singh P.C. & Hokada T. 2013: A new occurrence of sapphirine–spinel–corundum-bearing granulite from NE of Jagtiyal, Eastern Dharwar Craton, Andhra Pradesh. *Journal of Geoogical Society India* 82, 5–8. https://doi.org/10.1007/s12594-013-0115-6

Prakash D., Singh P.C. & Singh C.K. 2015: Reaction textures & metamorphic evolution of sapphirine–spinel-bearing & associated granulites from Diguva Sonaba, Eastern Ghats Mobile Belt, India. *Geological Magazine* 152, 316–340.

Prakash D., Singh P.C. & Tewari S. 2017: Petrology, pseudosection modelling & U–Pb geochronology of silica-deficient Mg–Al granulites from the Jagtiyal section of Karimnagar granulite terrane, northeastern Dharwar Craton, India. *Precambrian Research* 299, 177–194. https://doi.org/10.1016/j.precamres.2017.07.014

Prakash D., Yadav R., Tewari S., Frimmel H.E., Koglin N., Sachan H.K. & Yadav M.K. 2018: Geochronology & phase equilibria modelling of ultra-high temperature sapphirine+quartz-bearing granulite at Usilampatti, Madurai Block, Southern India. *Geological Journal* 53, 139–158. https://doi.org/10.1002/gj.2882

Prasad B.R., Rao G.K. & Mall D.M. 2007: Tectonic implications of seismic reflectivity pattern observed over the Precambrian Southern Granulite Terrain, India. *Precambrian Research* 153, 1–10. https://doi.org/10.1016/j.precamres.2006.11.008

Richardson S.W. 1968: Staurolite stability in a part of the system Fe–Al–Si–O–H. *Journal of Petrology* 9, 467–488.

Sajeev K., Osanai Y. & Santosh M. 2004: Ultrahigh-temperature metamorphism followed by two-stage decompression of garnet–orthopyroxene–sillimanite granulites from Ganguvarpatti, Madurai block, southern India. *Contributions to Mineralogy and Petrology* 148, 29–46. https://doi.org/10.1007/s00410-004-0592-0

Sandiford M. & McLaren S. 2006: Thermo-mechanical controls on heat production distributions and the long-term evolution of the continents. In: Brown M. & Rushmer T. (Eds.): Evolution and differentiation of the continental crust. *Cambridge University Press*, Cambridge, 67–91.

Sandiford M. & Powell R. 1986: Pyroxene exsolution in granulites from Fyfe Hills, Enderby L&, Antarctica: evidence for 1000 °C metamorphic temperatures in Archaean continental crust. *American Mineralogist* 71, 946–954.

Santosh M., Maruyama S. & Sato K. 2009: Anatomy of a Cambrian suture in Gondwana: Pacific-type orogeny in southern India? *Gondwana research* 16, 321–341. https://doi.org/10.1016/j.gr.2008.12.012

Santosh M., Yang Q. Y., Shaji E., Mohan M. R., Tsunogae T. & Satyanarayanan M. 2016: Oldest rocks from Peninsular India: Evidence for Hadean to Neoarchean crustal evolution. *Gondwana Research* 29, 105–135. https://doi.org/10.1016/j.gr.2014.11.003

Santosh M., Hu C.N., He X.F., Li S.S., Tsunogae T., Shaji E. & Indu G. 2017: Neoproterozoic arc magmatism in the southern Madurai block, India: Subduction, relamination, continental outbuilding, and the growth of Gondwana. *Gondwana Research* 45, 1–42. https://doi.org/10.1016/j.gr.2016.12.009

Santosh M., Tsunogae T., Yang C.X., Han Y.S., Hari K.R., Prasanth M.M. & Uthup S. 2020: The Bastar craton, central India: A window to Archean–Paleoproterozoic crustal evolution. *Gondwana Research* 79, 157–184. https://doi.org/10.1016/j.gr.2019.09.012

Sarvothaman H. 1984: Occurrences of sapphirine-bearing rocks near Jagtiyal, Karimnagar district, A. P. *The Quarterly Journal of the Geological, Mining & Metallurgical Society of India* 56, 202–207.

Sharma I.N. & Prakash D. 2007: Reaction textures and P–T conditions of Opx-Crd gneisses from Karimnagar, Andhra Pradesh, India. *Mineralogy and Petrology* 90, 175–197. https://doi.org/10.1007/s00710-006-0174-0

Sharma I.N. & Prakash D. 2008: A new occurrence of sapphirine-bearing granulite from Podur, &hra Pradesh, India. *Mineralogy and Petrology* 92, 415–425. https://doi.org/10.1007/s00710-007-0202-8

Sharma I.N. & Lal R.K., Mohan A. 2003: Chemographic relationship & metamorphic evolution of orthopyroxene or sillimanite-bearing garnetcordierite gneisses & sapphirine–spinel–corundum granulites from Karimnagar, NE part of the eastern Dharwar craton, India. *Memoirs – Geological Society of India* 52, 195–228.

Stüwe K. 2007: Geodynamics of the lithosphere: Quantitative description of Geological Problems. 2nd Edition, *Springer-Verlag*, Berlin, Heidelberg, Dordrecht, 1–493.

Subba Rao D.V., Charan S.N. & Narayana B.L. 1995: Symplectites in high-grade pelitic gneisses of Usilampatti Tamil Nadu: P–T conditions & geochemistry. *Journal of Geological Society India* 40, 37–45.

Subba Rao D.V., Nirmal Charan S. & Moeen S. 1997: A new occurrence of sapphirine in the high-grade Pelitic gneisses of Usilampatti, Tamil Nadu. *Journal of Geological Society, India* 49, 7–12.

Tang L., Santosh M., Tsunogae T., Koizumi T., Hu X. K. & Teng X. M. 2017: Petrology, phase equilibria modelling and zircon U–Pb geochronology of Paleoproterozoic mafic granulites from the Fuping Complex, North China Craton. *Journal of Metamorphic Geology* 35, 517–540. https://doi.org/10.1111/jmg.12243

Teale W., Collins A.S., Foden J., Payne J.L., Plavsa D., Chetty, T.R. K. & Fanning M. 2011: Cryogenian (~830 Ma) mafic magmatism and metamorphism in the northern Madurai Block, southern India: A magmatic link between Sri Lanka and Madagascar? *Journal of Asian Earth Sciences* 42, 223–233. https://doi.org/10.1016/j.jseaes.2011.04.006

Thompson A. B. & England P.C. 1984: Pressure-temperature time paths of regional metamorphism II: their inference & interpretation using mineral assemblages in metamorphic rocks. *Journal of Petrology* 25, 929–954.

Topuz G. & Altherr R. 2004: Pervasive rehydration of granulites during exhumation–an example from the Pulur complex, Eastern Pontides, Turkey. *Mineralogy and Petrology* 81, 165–185. https://doi.org/10.1007/s00710-003-0034-0

Tsunogae T., Santosh M. & Ohyama H. 2008: High-pressure and ultrahigh-temperature metamorphism at Komateri, Northern Madurai Block, Southern India. *Journal of Asian Earth Sciences* 33, 395–413.

Wetherill G.W. 1956: Discordant uranium lead ages. *Eos, Transactions American Geophysical Union* 37, 320–326. https://doi.org/10.1029/TR037i003p00320

White R.W., Powell R. & Holland T.J.B. 2014: New mineral activity-composition relations for thermodynamic calculations in metapelitic systems. *Journal of Metamorphic Geology* 32, 261–286. https://doi.org/10.1111/jmg.12071

Whitney D.L. & Evans B.E. 2010: Abbrevatiations for names of rock-forming minerals. *American Mineralogist* 95, 185–187. https://doi.org/10.2138/am.2010.3371

Whittington A.G., Hofmeister A.M. & Nabelek P.I. 2009: Temperature-dependent thermal diffusivity of the earth's crust and implications for magmatism. *Nature* 458, 319–321. https://doi.org/10.1038/nature07818